

HIGH REYNOLDS NUMBER AIRFOIL: FROM WALL-RESOLVED TO WALL-MODELED LES

A. Frère^{1,2}, K. Hillewaert¹, P. Chatelain², G. Winckelmans²

A. Frère : ariane.frere@cenaero.be

K. Hillewaert : koen.hillewaert@cenaero.be

P. Chatelain : philippe.chatelain@uclouvain.be

G. Winckelmans : gregoire.winckelmans@uclouvain.be

1. *Cenaero, Gosselies, Belgium*

2. *Institute of Mechanics, Materials and Civil Engineering (iMMC), Université catholique de Louvain (UCL), Louvain-la-Neuve, Belgium*

Abstract

This paper presents an in-depth study, using wall-resolved Large-Eddy Simulation (wrLES), of a high Reynolds number airfoil in a near-stall condition. The flow around the NACA4412 airfoil, a widely used test case for turbulence modeling validation, is computed at Reynolds number $Re = 1.64 \times 10^6$ and angle of attack $\alpha = 12^\circ$. In the first part of the paper, the results are compared to previous experimental and numerical results, showing close agreement with both. In order to aid wall-model development, the second part of the paper characterizes the effect of the adverse pressure-gradient (APG) on the turbulent boundary layer development, and evaluates different wall-models in an a priori manner. It appears that the simple models, which assume an equilibrium flow, provide a better match to the mean flow velocity than allegedly more advanced models. The study reveals also that the often used simplification of the “Two-Layer Model” (TLM) that takes the pressure-gradient into account but neglects the convective terms, is not adequate. This simplification applied to the TLM indeed leads to a higher error than the simple equilibrium models. Therefore, it is argued that if the convective terms are neglected, the pressure-gradient term needs to be neglected as well.

Keywords

Large-eddy simulations, Wall-model, Adverse pressure-gradient, Boundary layer, NACA4412 airfoil

1 Introduction

Large-Eddy Simulation (LES) of wall-bounded flows at the Reynolds numbers that are relevant for wind turbine, turbomachinery or aircraft design ($Re \geq 10^6$) currently requires too much resources to be used in practice. However, as LES can provide more physical insights and higher fidelity than the currently affordable modeling approaches, it is needed by the industry. Therefore, cost reduction is of high importance. Wall-modeled LES (wmLES) alleviates the LES near-wall grid requirement by employing a wall-

model to reconstruct the wall shear stress based on data taken further away from the wall. In this way, wmLES is seen as a promising solution towards computation of high Reynolds number flows. wmLES techniques have demonstrated high accuracy on test cases such as the turbulent channel flow [1–5]. However, the results are currently unsatisfactory for cases presenting an adverse pressure-gradient (APG).

A first obstacle towards developing reliable wmLES is the lack of perfectly reproducible validation test cases

Four recent studies [6–9] attempted the validation of wmLES approaches by simulating the flow over the NACA4412 airfoil, see Fig. 1. In all cases, the overall flow was captured but there were still differences with the experimental reference case. These differences could be due to an inability of the wall-models to capture the APG. However, all authors put forward the difficulty, or even the incapacity, to exactly reproduce the experimental conditions. In particular, the trip wire could not be reproduced considering the coarse near wall-grid used with wall-models [6, 8, 9]. Furthermore, the study that obtained the best match with the experiment [8] was also the only one to model the effect of the wind tunnel blockage.

Whatever the actual origin of the observed differences, it is clear that the inherent difference between the experimental and the numerical setup leads to difficulties in developing and validating the wall-model approaches. Therefore, the ideal wmLES validation case should be a wall-resolved LES or even a Direct Numerical Simulation (DNS) run under exactly the same conditions as the wmLES.

Unfortunately, due to their high computational cost, most of the numerical reference cases (wrLES, DNS) concern Reynolds numbers that are too low to be relevant for wmLES validation. The reason is highlighted in Fig. 2, which shows the impact of an APG on the boundary layer development over the same bump geometry for two Reynolds numbers. The bump was designed by Dassault Aviation to reproduce a typical APG observed on an airfoil at high angle of attack [11]. The test case was studied first experimentally at $Re_c = 6500$ [11] and then reproduced by DNS at the highest accessible Reynolds number, namely $Re_c = 395$ [12]. Figure 2 provides the pressure coefficient evolutions over the bump for the two Reynolds numbers. In both cases, the bump induces first a favorable pressure-gradient until the top of the bump where $C_p \simeq 1.5$ but the adverse pressure-gradient is slightly different with, at low Reynolds number, a plateau that reveals a separated region. The boundary layer velocity profiles are shown for both Reynolds numbers at different positions in the adverse pressure-gradient region. The profiles are given in wall units¹. At the higher Reynolds number, a common log-layer region is observed in all of the profiles, effectively decoupling the outer layer, highly impacted by the APG, from the inner layer. The latter appears to behave in an universal way, usually referred to as “the law of the wall” with $u^+ = f(y^+)$.

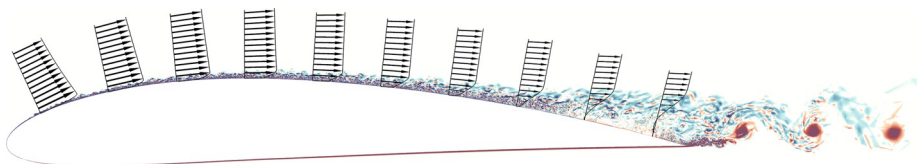


Fig. 1 Mean velocity profiles and instantaneous spanwise vorticity over the NACA4412 airfoil at $\alpha = 12^\circ$ and $Re = 1.64 \times 10^6$

¹ *i.e.* using the local wall shear stress $\tau_\omega = \rho u_\tau^2$ to non-dimensionalize the tangential velocity $u^+ = u/u_\tau$ and the normal wall distance $y^+ = yu_\tau / \nu$ with ν the kinematic viscosity.

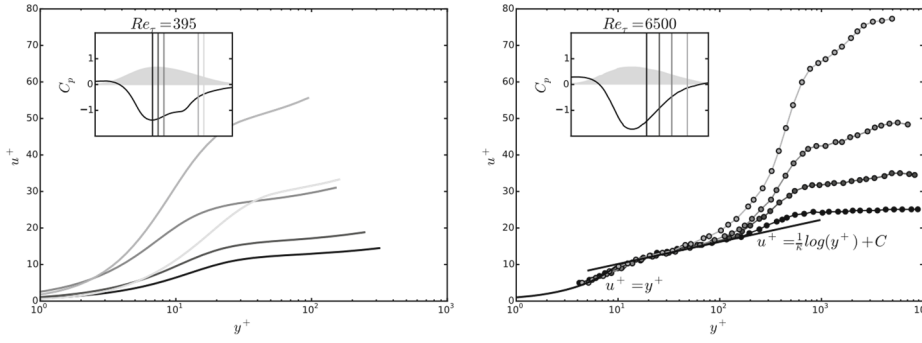


Fig. 2 Impact of an adverse pressure-gradient at low and high Reynolds numbers. The small figure presents the geometry (gray area), the pressure coefficient (black curve) and the locations corresponding to the velocity profiles plotted in the main figure (vertical lines colored from black to gray). The low Reynolds number results are on the left (the data come from the DNS database [10] and have been analyzed by the author). The experimental high Reynolds number results are on the right (the data have been extracted by the author from Bernard et al. [11])

At the lower Reynolds number, there is no logarithmic layer, and the impact of the APG goes up to the wall. A wall-model developed and/or validated on the basis of low Reynolds number data is therefore likely not applicable to high Reynolds number cases; and conversely. Therefore, numerical reference cases at high Reynolds numbers are highly desirable for the development of wmLES.

A second obstacle is the lack of consensus on the appropriate wall-models

The most basic wall-models are based on analytical laws that provide a direct link between the velocity u (and potentially other data such as the pressure-gradient) at a pre-specified distance y from the wall and the wall shear stress τ_w . A widely used expression is the Reichardt law-of-the-wall [13]

$$u^+ = \frac{1}{\kappa} \ln(1 + \kappa y^+) + \left(C - \frac{1}{\kappa} \ln(\kappa) \right) \left(1 - e^{-\frac{y^+}{11}} - \frac{y^+}{11} e^{-\frac{y^+}{3}} \right), \quad (1)$$

where κ and C are two coefficients. Their value is the subject of many works in the literature but here $\kappa = 0.38$ and $C = 4.1$ are used, as suggested by the more recent works. Another wall-model, which is used by commercial codes (e.g. [14]), is the Werner and Wengle formula [15]. This model has the advantage of providing the wall shear stress without requiring to solve a non-linear equation

$$|\tau_w| = \begin{cases} \frac{2\mu|u_m|}{y_{wm}} & u_m \leq \frac{\mu}{2\rho y_{wm}} A^{\frac{2}{1-B}} \\ \rho \left[\frac{1-B}{2} A^{\frac{1+B}{1-B}} \left(\frac{\mu}{\rho y_{wm}} \right)^B |u_m| \right]^{\frac{2}{1+B}} & u_m > \frac{\mu}{2\rho y_{wm}} A^{\frac{2}{1-B}}. \end{cases} \quad (2)$$

In this expression, u_m is the averaged velocity between the wall and the wall-model input location y_{wm} , ρ is the density and μ is the dynamic viscosity. A and B are two coefficients taken as $A = 8.3$ and $B = 1/7$ [14].

Although these two laws are dedicated to equilibrium flows, they should also be applicable to APG as long as the boundary layer velocity profile features a log-layer region and as the wall-model input is before the end of that region. However, many authors have developed more elaborate expressions that explicitly take the APG into account. Brionnaud et al. obtained promising results on a detached flow over an aircraft wing [16] using the ‘‘Generalized law-of-the-wall’’ of Shih [17]

$$u = \frac{\tau_\omega}{|\tau_\omega|} u_\tau f_1(y^+) + \frac{p^+}{|p^+|} u_\tau p^{+\frac{1}{3}} f_2\left(y^+ p^{+\frac{1}{3}}\right) \quad (3)$$

Where $\rho^+ = \frac{v}{\rho u_\tau^2} \frac{dp}{dx}$ is the pressure gradient in wall units and f_1 and f_2 are calibrated fifth-order polynomials.

This approach is interesting as it has basically the same cost as the classical Reichardt model.

However, the most widely used model is the “Two-Layer Model” (TLM) of Balaras et al. [18] that couples LES to simplified RANS equations

$$\left(\frac{\partial^2 u^+}{\partial y^{+2}} + \frac{\partial(-\overline{u'v'})^+}{\partial y^+} \right) = \{p^+\} + \left[u^+ \frac{\partial u^+}{\partial x^+} + v^+ \frac{\partial u^+}{\partial y^+} \right]. \quad (4)$$

In its full form, the model is computationally more expensive since it requires the solution of these equations on an auxiliary, boundary fitted grid. It is therefore often simplified. The most frequent simplification neglects the convective terms [19], indicated by the straight brackets. However, a recent review by Larsson et al. [4], states that the convective terms approximately balance the pressure-gradient term (term within curly brackets), such that both should either be considered or neglected together.

The present project aims at performing a wrLES of the NACA4412 at $Re = 1.64 \times 10^6$ and $\alpha = 12$ in order to compare different widely used wall-models a priori

The steps of the study consist of

- providing a numerical reference, which can be reproduced, for the validation of wmLES or related approaches;
- extracting from this database the quantities used as wall-model in- and outputs;
- using these quantities to assess the validity of various existing wall-models.

Instead of comparing the different models a posteriori by analyzing the results of different wmLES computations, the models will be confronted here in an a priori manner on the basis of a wall-resolved LES. The focus of the comparison presented in this paper is on evaluating the models capacity to represent APG effects and, more specifically, on answering the following questions:

1. Can an analytical approach that assumes equilibrium match velocity profiles in APG boundary layers at high Reynolds number?
2. How does the use of Reichardt equilibrium law-of-the-wall compare to that of Werner and Wengle’s model?
3. Does the use of the analytical model of Shih [17], which explicitly includes the pressure-gradient, improve upon that of the equilibrium law?
4. Can the more advanced and expensive “Two-Layer Model” [18] be simplified by removing the convective and/or the pressure-gradient terms?

The paper is organized as follows. Section 2 describes the CFD methodology and the computational setup. Section 3 compares the wrLES results to seven previous numerical and experimental studies. Section 4 uses the wrLES results to characterize a flow submitted to an APG. Finally, Section 5 compares the different wall-models to address, in Section 6, the questions raised above.

2 CFD Methodology and Computational Setup

The simulations are performed using the high order Discontinuous Galerkin method (DGM). This method provides accuracy, low dissipation and low dispersion irrespective of the mesh type. It is furthermore highly scalable and is thus well adapted for LES of large-scale industrial applications [20]. Argo, the DGM code used in this study, solves the compressible Navier-Stokes equations using an Implicit LES (ILES) approach, in which the subgrid scale dissipation is provided by the numerical scheme. Argo has been successfully

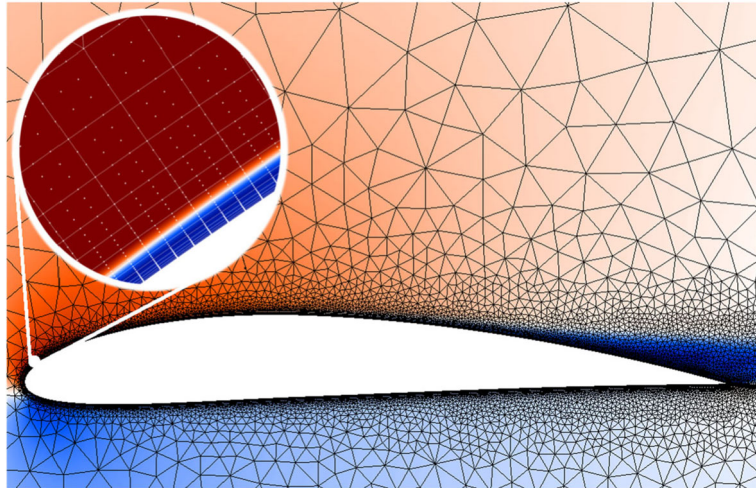


Fig. 3 View of the 2D unstructured mesh on the top of the time- and span-averaged velocity magnitude. Quadrangles are used in the boundary layer and triangles in the far field. The small inset gives a zoom on the laminar separation bubble. The white markers represent the position of the interpolation points in the fourth order accurate ($p = 3$) elements. In the zoom, there are about seven elements in the thickness of the blue region

validated on DNS and ILES of academic and industrial benchmarks such as the Taylor-Green vortex [21], the turbulent channel flow and several low Reynolds number airfoils [22, 23]. Over the past few years, wall-models have been added. Promising results have been obtained on the turbulent channel flow test case [24] and the wmLES approach has hence been tested on the NACA4412 [7].

The wrLES computation is performed at $\alpha = 12^\circ$ and $Re = 1.64 \times 10^5$ on a 2D mixed-element mesh, extruded in the spanwise direction. No turbulence is introduced at the inlet and the flow conditions are chosen such that the freestream Mach number equals 0.09. The geometry and the 2D grid were created using Gmsh [25]. The original NACA4412 airfoil shape was slightly modified to obtain a sharp trailing edge as described in the NASA 2DN44 benchmark [26].

The 2D grid consists in a C-type mesh with quadrangle in the boundary layer and triangles in the far-field. The structured wall-normal mesh consists of 13 layers with a first layer thickness of $2.5 \times 10^{-5}c$ and a total thickness of about $5 \times 10^{-3}c$. Unlike the wall-normal mesh that is uniform through the chord, the streamwise resolution varies with, in total, 1170 points used around the airfoil. The 2D mesh is presented in Fig. 3. High-order polynomials interpolate the solution within each cell of the domain. Cubic polynomials ($p = 3$) are considered in this work as these are optimal for the present DG method [28], leading to fourth-order accurate elements. Therefore, each quadrangle and triangle count 16 and 10 interpolation nodes, respectively. The interpolation nodes are illustrated in the zoom of Fig. 3.

To use refinement criteria that are comparable to the finite volume and finite difference ones, each distance of the physical mesh is divided by $p = 3$. One then speaks about *effective* resolution. This gives an effective

wall-normal mesh growth rate of about 1.1 that is in line with the DG best practices [29] and the effective streamwise (x), wall-normal (y) and spanwise (z) resolutions that are presented in Fig. 4. These refinements are in agreement with Choi and Moin's guidelines [27], *i.e.* $\Delta x^+ \simeq 50 - 130$, $\Delta y^+ \simeq 1$ and $\Delta z^+ \simeq 15 - 30$

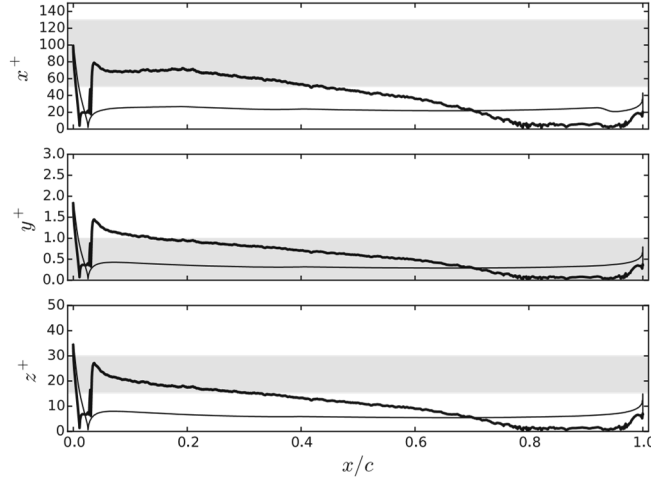


Fig. 4 Chordwise wall-refinement in the streamwise (x), normal (y) and spanwise (z) directions. The wrLES results (black) are compared to Choi and Moin guidelines [27] (gray area). The suction side data are highlighted by using a thicker line

Besides the thirteen structured layers around the airfoil, the mesh is unstructured and has been coarsened rapidly to limit the required computational resources. Therefore, although the refinement is sufficient near the wall, it might be slightly too coarse to capture the full boundary-layer height.

The use of the unstructured mesh makes possible to obtain a rapid increase of the element size and to reduce the grid cost, allowing to fix the far-field conditions at a distance of more than 10 chords. However, due to computational restrictions, the span extent was limited to $\sim 1\%$ of the chord. The spanwise mesh consists precisely of 22 layers of uniform thickness leading to a total span extent of $x/c = 0.010312$. The total 3D mesh counts $\sim 0.6 \times 10^6$ elements and, as cubic polynomials are used, this leads to $\sim 35 \times 10^6$ degrees of freedom. The use of this narrow span leads to two-dimensional near-wake vortices, as can be observed in Fig. 1.

Figure 5 presents the evolution of the three characteristic boundary layer thicknesses and compare them to the measurements of Wadcock [30]. It appears that, although the span extent is $s/c \simeq 0.01$, the computed boundary layer evolution is similar to the experimental one up to $x/c \simeq 0.5$ where $\delta/c \simeq 0.015$. After that point, the evolution remains qualitatively similar, although it is quantitatively different. It also appears that the computed displacement and momentum thicknesses are similar to the experimental one up to $x/c \simeq 0.7$. Therefore, this wrLES is considered already sufficient for the purpose of investigating a priori wall models for LES and validating them, at least up to $x/c \simeq 0.6 - 0.7$

A second order accurate backward difference implicit time integration is used, with a timestep non-dimensionalized using the flow-through time ($ftt = c/u_\infty$) as $\Delta t/ftt = 2.2 \times 10^{-4}$. Starting from a statistically converged computation using $\nu = 2$, the computation was run over eight additional flow-through times to evacuate the transient, leading to a variation of the time-averaged lift coefficient over one ftt that is less than 0.5%. Then time- and spanwise-averaged statistics were obtained during two additional flow-through times. This time-frame is considered as sufficient as the second order statistics do not vary anymore. The computations have been performed on Ivybridge nodes and one flow-through time required about 0.3 MioCPUh.

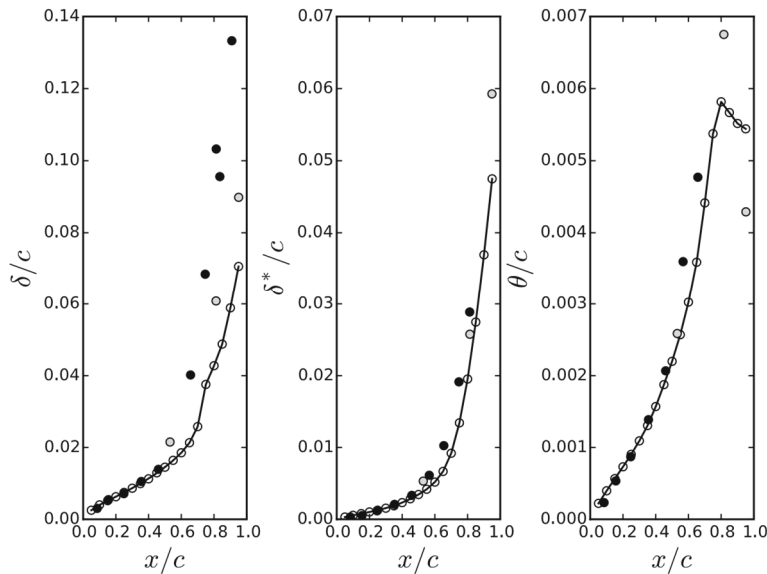


Fig. 5 Chordwise evolution of the boundary layer parameters. Boundary layer thickness (left), displacement thickness (center) and momentum thickness (right). The experimental results obtained by Wadcock [30] with two different measurement techniques are also provided for comparison (black and gray circles)

3 Comparison to Previous Studies

The wrLES results are compared to two experiments [30, 31], four wall-resolved LES [32–35] and one wall-modeled LES [8]. All studies used in the comparison have been performed at $Re = 1.64 \times 10^6$ and $\alpha = 12.0^\circ$. However, the computational configurations differ in some aspects that are summarized in Table 1. The aim of this section is essentially to discuss the impact of these different configurations.

The configurations are differentiated in Table 1 based on three important setups: the forcing of the transition, the modeling of the wind tunnel blockage and the span extent. As the flow statistics are averaged over the time and the span, it would be interesting to also add the number of *ftt* considered in the statistics. However, this information is rarely provided, or it is not complete. For example, Kaltenbach and Choi [34] mention the use of 2 *ftt* for the statistics, but do not precise how is the calculation initialized and how many *ftt* are needed to evacuate the transient. Schmidt et al. [35] specify only an entire computation time of 8 *ftt*. Park and Moin [8] mention the use of 12 *ftt* to evacuate the transient, followed by 4 *ftt* for the statistics. Furthermore, in an equivalent study performed on the DU96 airfoil ($Re = 1.5 \times 10^6$, $\alpha = 10.3^\circ$ and $s/c = 12\%$), Venugopal et al. [36] initialize the calculation based on a 2D computation; they then use 2.6 *ftt* to evacuate the transient and 1 *ftt* for the statistics. Therefore, there is no clear trend, nor common practice in the literature. This is due to the fact that these times are, unfortunately, largely depending on the available computational resource. With limited resource, some groups decide to reduce the transient phase, other groups decide to reduce the statistics time. In this work, a large transient time was use to be certain to reach the convergence. A shorter time was then used for the statistics. It appears, however, that this time is sufficient to have converged statistics, as discussed in Section 2.

The most important flow features are to be found along the suction side. Close to the leading-edge, the thin laminar boundary layer separates and then reattaches, creating a laminar separation bubble (LSB). Further downstream, the now turbulent boundary layer grows under the effect of the APG and finally separates at about 80% of the chord.

Table 1 Summary of the different set-ups considered in the comparison of Section 3

	Type	Forced transition	Tunnel blockage	Span extent as % chord
Wadcock [30]	exp.	yes	yes	280%
Hasting and Williams [31]	exp.	yes	yes	400%
Kaltenbach and Choi [34]	wrLES	yes	no	2.5 – 5%
Jansen [32]	wrLES	no	no	2.5 – 5%
Jansen [33]	wrLES	yes	yes	2.5 – 5%
Schmidt et al. [35]	wrLES	yes	no	5%
Park and Moin [8]	wmLES	no	yes	72%
Current work	wrLES	no	no	1%

To compare the current computation to the different studies, it is interesting to examine the chordwise pressure and friction coefficient evolutions as well as the velocity profiles.

Pressure and friction coefficients

Figure 6 presents the chordwise pressure coefficient obtained by the different studies. As the experimental pressure curve obtained by Hasting and Williams [31] is very similar to the one obtained by Wadcock [30], only the latter is shown on this figure. From this comparison, it appears that the present simulation is within the range of the previous studies and matches the experimental reference well.

A close look on the last 20% of the chord shows that the pressure plateau observed in the experiment is rarely captured numerically. For example, Jansen's wrLES from 1995 does not present a plateau. In 1996, Jansen showed that considering the tunnel blockage helped in obtaining a pressure plateau [33]. This seems to be confirmed by the wmLES from Park and Moin [8]: they considered the blockage and they obtained a plateau matching the experimental one.

However, although the wrLES performed with Argo does not consider the blockage, it captures well the plateau. Jansen [32] compared two span extents of 2.5%c and 5%c and observed that the narrow span artificially leads to a pressure plateau closer to the experiment. However, as his comparison was made using two different grid refinements, he added that no strong conclusion could be drawn.

The same year, Kaltenbach and Choi [34] compared the two same span extents while keeping the refinement constant and concluded that the span extent was not impacting the C_p curve. Therefore, the impact of the span is not clear and this new wrLES might be artificially close to the experiment only due to its narrow span extent. However, as mentioned previously, the goal of the present computation is to be reproducible using a wmLES approach, and not to match the experimental data beyond the separation of the boundary layer.

Further interesting information can be inferred from the evolution of the friction coefficient along the airfoil, presented on Fig. 7. One notices that the wrLES results contain two separated regions. The first separation region, corresponding to the LSB, starts at $x/c = 0.01$ and reattaches at $x/c = 0.03$. After $x/c = 0.76$, a relatively large zone of near zero C_f is observed, before an actual separation (*i.e.* with C_f clearly negative) that occurs at about $x/c = 0.97$.

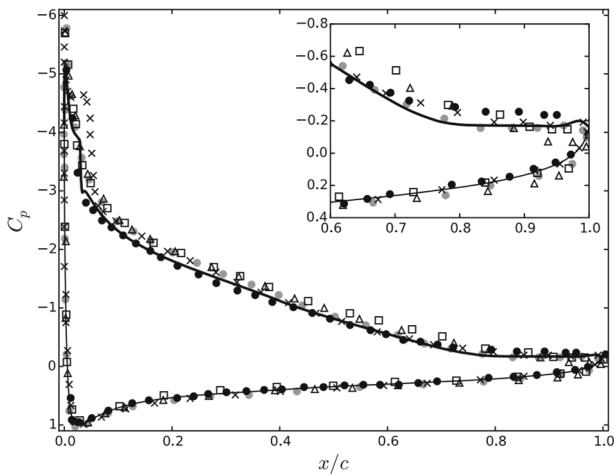


Fig. 6 Chordwise pressure coefficient evolution. Different wmLES and wrLES are compared to Wadcock's experiment (black circles) [30] and to the present wrLES (solid black line): Kaltenbach and Choi (squares) [34], Jansen (triangles) [32], Schmidt et al. (crosses) [35] and Park and Moin (gray circles) [8]. For the current wrLES, the suction side data are highlighted by using a thicker line. Except for the present wrLES, all data have been digitized manually based on the reference papers

Transition through laminar separation bubble

In the experiment, the transition is forced using boundary layer tripping on both the suction and pressure sides. Given modeling ambiguity and the artificial nature of such a device, the tripping is not considered in the present computation. Nevertheless, transition occurs on the suction side almost exactly at the same position as in the experiment.

In all previous studies where transition is not forced, the authors observe an LSB at the leading edge. However, only Jansen characterizes it by providing the velocity profiles in that region [32]. Furthermore, Hasting and William [31] mentioned that they did a few tests without tripping and observed, at an angle near stall, an LSB spanning between 1 and 1.7% of the chord. Figure 8 provides a visualization of the LSB as well as a comparison of the tangential velocity profile in the LSB region.

Although Jansen used the terms "coarse" and "fine" to differentiate between his two meshes, they are called here "a" and "b" because the "fine" mesh has been run on a twice narrower span; so the origin of the small differences is not clear. Therefore, the two cases are seen here only as two different computations.

The comparison shows that all simulations present an LSB in the region $0.01 \leq x/c \leq 0.05$ and that the maximum thickness observed is $\approx c / 1000$. Although this thickness is small, it is well captured by the wall-normal grid as it corresponds to about eight fourth order elements. At $x/c = 0.02$, the LSB thickness obtained by the mesh b is twice bigger than the one obtained by the two other wrLES. However, already at $x/c = 0.04$, the velocity obtained with mesh b is almost identical to the one from the current wrLES. As the differences between the three wrLES are small in absolute value, it is concluded from this comparison that the three wrLES have globally the same LSB.

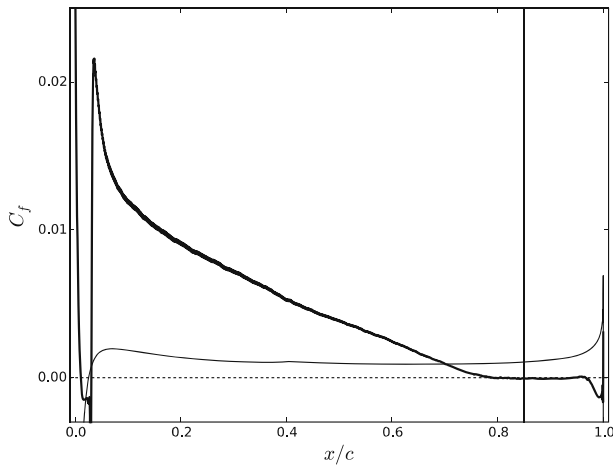


Fig. 7 Chordwise friction coefficient evolution. Argo wrLES friction coefficient (black curve) is compared to the separation point measured by Wadcock (vertical black line). The suction side data are highlighted by using a thicker line

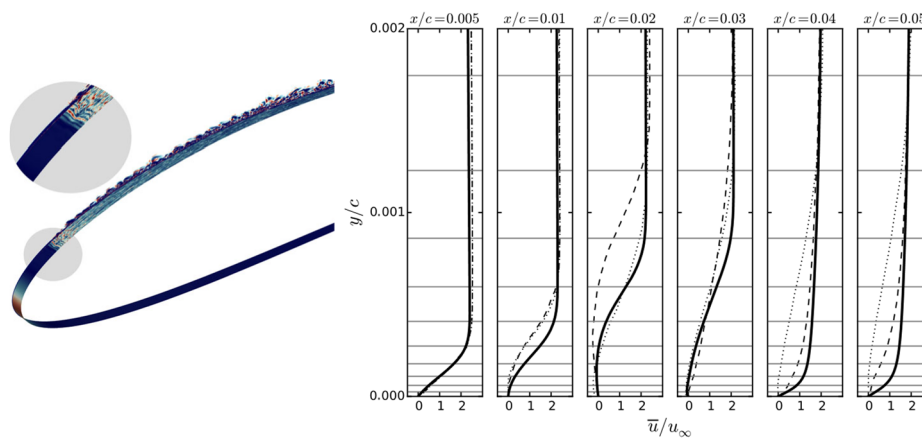


Fig. 8 Characterization of the laminar separation bubble. A view of the instantaneous shear on the airfoil surface and of the instantaneous spanwise vorticity is given on the left. A comparison of the tangential velocity profiles along the chord is given on the right. The results (solid line) are compared to the two previous wrLES from [32], on mesh a (dotted) and mesh b (dashed). The horizontal gray lines represent the wall normal grid refinement

4 Characterization of the Boundary Layer Subject to an APG

This section presents the evolution of the boundary layer thickness, the velocity and the Reynolds stresses on the suction side of the airfoil with a focus on the region subject to the APG, before the separation. Figure 9 shows the evolution of the tangential velocity along the chord at positions x/c ranging from 0.05 to 0.95 with steps of 0.05. On the global view, the deceleration of the flow is observed with a maximum edge velocity $u / u_{\infty} \approx 2$ at $x/c = 0.05$ that reduces to $u / u_{\infty} \approx 1$ after $x/c \geq 0.7$. The growth of the boundary layer thickness is also observed, ranging from $\delta/c \approx 0.005$ at $x/c = 0.05$ to $\delta/c \approx 0.03$ at $x/c = 0.7$. The negative slope obtained for $x/c \geq 0.85$ indicates that the flow is separated in that region. However, the friction coefficient presented previously in Fig. 7 shows a large region with essentially zero friction coefficient ranging within $0.77 \leq x/c \leq 0.97$. Therefore, a closed view of Fig. 9 is also provided to visualize the slopes at the wall. This confirms that, for all profiles with $0.75 \leq x/c \leq 0.95$, the slope, and thus the friction, is negligible.

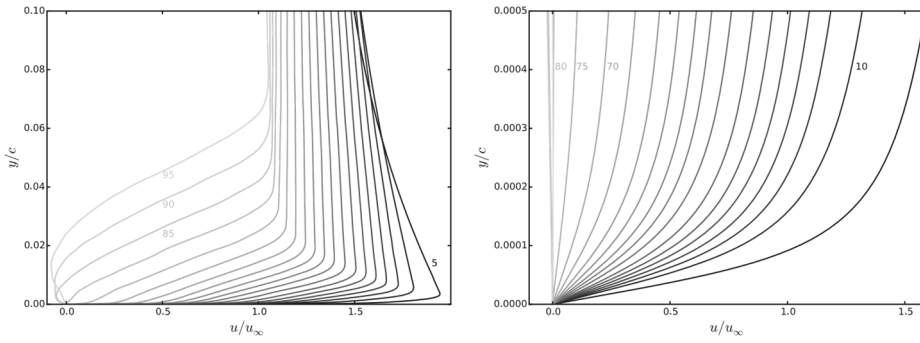


Fig. 9 Tangential velocity profile evolutions along the chord. The profiles are given at positions x/c ranging from 0.05 to 0.95 with steps of 0.05 and are colored from black to light gray. A global view is given on the left. A closed view of the near-wall region is given on the right

The non-separated velocity profiles of Fig. 9 are also presented on Fig. 10 in wall units and logarithmic scale. It appears that all curves collapse in the viscous sublayer and in a part of the logarithmic region ($y^+ \leq 100$), to separate in the wake region.

In Fig. 11, the pressure gradient term is expressed using both its value in wall units p^+ as well as the Clauser parameter $\beta = \delta^* \frac{dp/dx}{\tau_w}$. As these two go to infinity at the separation, they are presented up to $x/c = 0.75$, where $p^+ \simeq 0.4$ and $\beta \simeq 100$. Vinuesa et al. [37] studied the NACA4412 airfoil by DNS at a lower angle of attack and a lower Reynolds number ($Re = 4 \times 10^5$ and $\alpha = 5^\circ$). They studied the chordwise evolution of β and obtained an evolution similar to our result with a maximum value $\beta = 87$. In their case, this maximum is obtained close to the trailing edge, at $x/c = 0.98$, hence indicating that no separation occurred. Vinuesa et al. observed a strong increase of the Reynolds stresses and the apparition of a second peak in the streamwise fluctuation profile. Figure 12 performs the same evaluation as in Vinuesa et al.'s work and a similar behavior is observed. Note that, for the sections where $y^+ \geq 100$, some oscillations appear, and they are bigger for large x/c . These are due to the fact that the mesh is too coarse in that region, as discussed in Section 2.

5 Comparison to Different Wall-Model Estimates

The common approach for comparing different wall-models consists in performing multiple wmLES. An alternative approach, used in the current study, evaluates the models (Reichardt (1), Werner and Wengle (2), Shih (3) and TLM (4)), in an a priori manner using the wrLES data. The procedure is the following:

1. the wall-model inputs ($u(y_{wm}), dp/dx$) are interpolated in the wrLES results;
2. the wall shear stress is computed following the model;
3. the wall-model is assessed by comparing the predicted shear stresses and corresponding velocity profiles to the wrLES results.

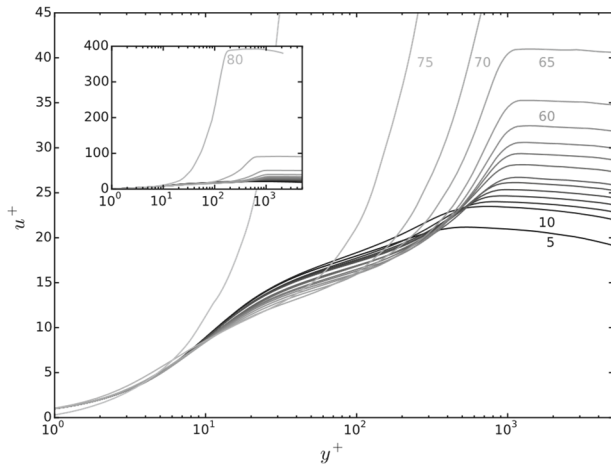


Fig.10 Tangential velocity profile evolutions along the chord in wall units and logarithmic scale. The profiles are given at positions x/c ranging from 0.05 to 0.80 with steps of 0.05 and are colored from black to light gray. The small figure presents the global view. The main figure gives a closed view

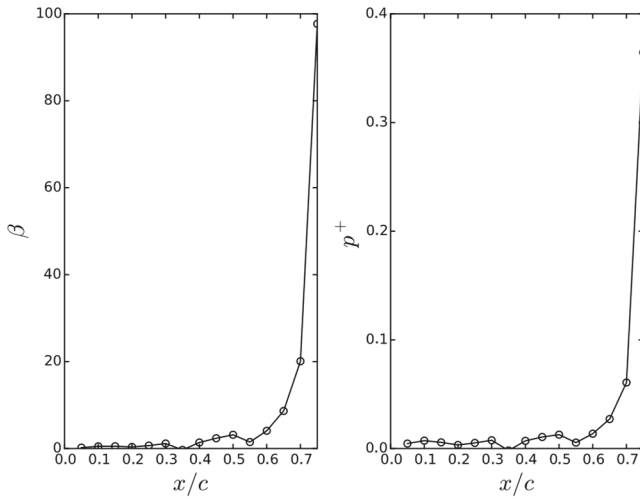


Fig. 11 Chordwise evolution of the pressure-gradient terms characterizing the boundary layer: Clauser parameter β (left) and p^+ (right)

This analysis is undertaken for three different positions along the chord and before the separation region, namely $x/c = 0.2, 0.5, 0.7$, and for five different wall-model input positions, namely $y_{wm}/c = 0.1, 3, 6, 9, 11 \times 10^{-3}$. For the TLM model, two laws are used. The first one, called TLMdp neglects the convective terms. The second one, called TLMequi

neglects both convective and pressure-gradient terms. In both case, the following relation is used

$$\frac{v_t}{v} \frac{\partial u^+}{\partial y^+} = -\overline{u'v'} \quad (5)$$

and the turbulent viscosity is approximated by $v_t/v = \kappa y^+(1 - \exp(-y^+/19))^2$ as used in [38, 39].

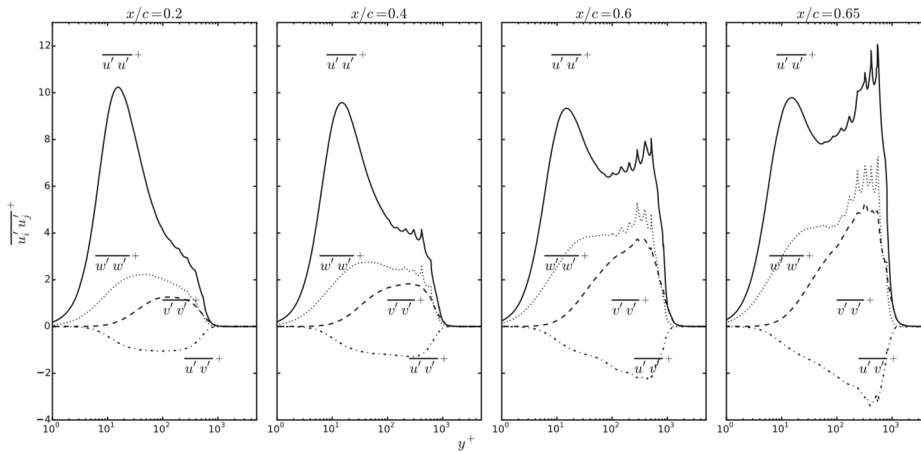


Fig. 12 Reynolds stresses along the suction side of the airfoil for different chordwise positions. All subfigures presents from top to bottom, the streamwise $\overline{u'u'}$ (solid), spanwise $\overline{w'w'}$ (dotted), normal $\overline{v'v'}$ (dashed) velocity fluctuations and, in negative, the Reynolds shear stresses $\overline{u'v'}$ (dash-dotted)

Figure 13 compares the velocity profiles estimated by the wall-models to the wrLES database at the three chordwise locations. As Werner and Wengle's model provides the shear stress directly, without passing by an estimate of the velocity profile, only the four other models are compared here.

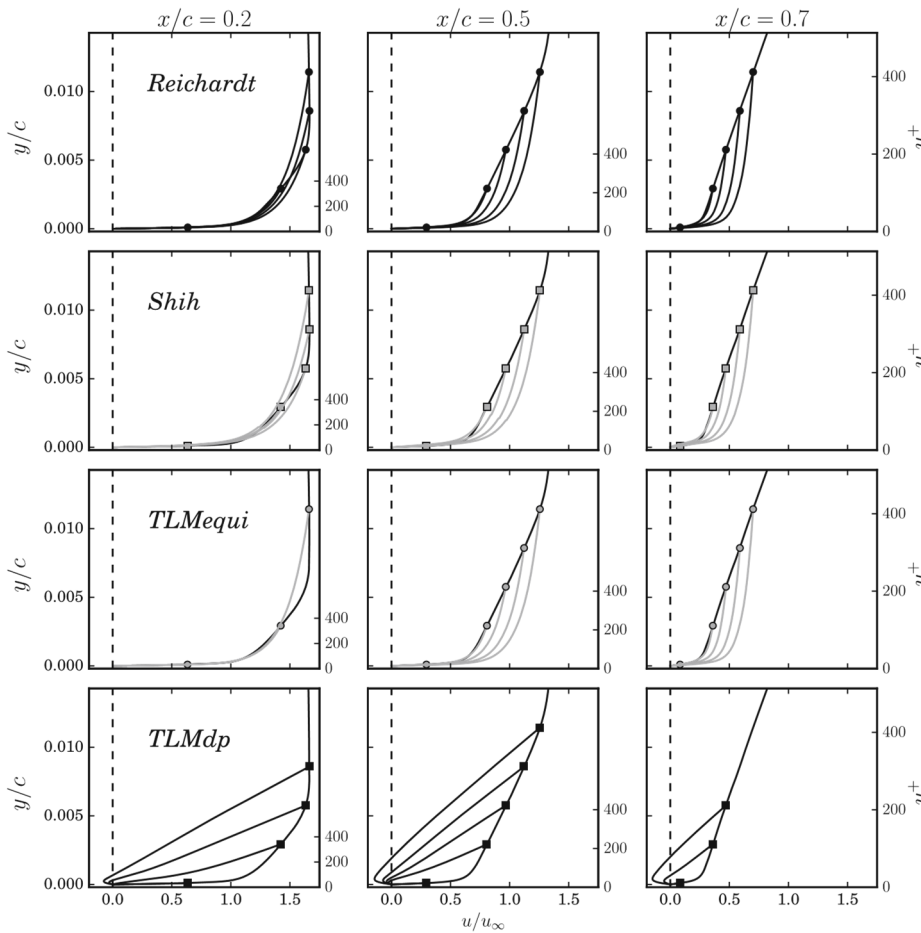


Fig. 13 Comparison in the physical scale of the velocity profiles estimated by the wall-models to the wrLES data (solid black line) at three different chordwise locations. Four models are compared with from top to bottom Reichardt, Shih, TLMequi and TLMdp. The markers show the position of the wall-model input. Wallmodels that assume an equilibrium state are marked by circles with Reichardt (black) and TLMequi (gray). Wall-models that add the contribution of the pressure-gradient are marked by squares with Shih (gray) and TLMdp (black)

For each chordwise location and wall-model, a sub-figure shows the velocity profiles obtained for the five input locations. If, for one input location, the model did not converge, no profile is given. One sees that Reichardt and Shih's models always converged, and that more troubles were encountered for the two TLM simplifications. For all models, a simple Newton iteration was used. A more advanced algorithm would definitely permit to obtain convergence of all models. However, this constitutes an interesting example of the complexity added by the models that are not based on simple algebraic relations. Each sub-figure also provides the wall-distance in y/c and y^+ defined based on the wrLES wall shear stress. Recall that the wall-model input positions are at constant y/c for the three chordwise locations and not at constant y^+ . This choice is deliberate, as the common meshing practice typically uses a constant wall-normal grid size along the chord.

Figure 13 shows that the TLM variant that neglects both the convective and the pressuregradient terms (TLMequi) is matching better the wrLES reference than the alleged more advanced variant that neglects only the convective terms (TLMdp). Already at $x/c = 0.2$, the TLMdp estimates that the flow separates. This model thus appears to overestimate the impact of the APG. On this figure, the difference between Reichardt, Shih and TLMequi models is not distinguishable. Therefore, Fig. 14 compares the three models in wall units and in logarithmic scale. As Reichardt and TLMequi's laws are defined as a relation between u^+ and y^+ only, the curves at the three chordwise locations are similar. As Shih's law takes also p^+ into account, the curve deviates from Reichardt's curve for increasing p^+ and x/c . It appears that Reichardt and TLMequi's laws provide a good estimate as long as the input position is placed on the log-region. In the most restrictive case, that is at $x/c = 0.7$, the log region ends at $y^+ \approx 100$. So as long as the input $y_{wm}^+ \leq 100$, Reichardt and TLMequi's models should be correct. Again, the alleged more advanced model, that is here Shih's law, appears to be further from the wrLES. Shih's law does not produce a common log-region, as if the APG impact was overestimated or as if the model was made to capture a lower Reynolds number flow. Shih's model appears therefore not adapted to the flow physics concerned here.

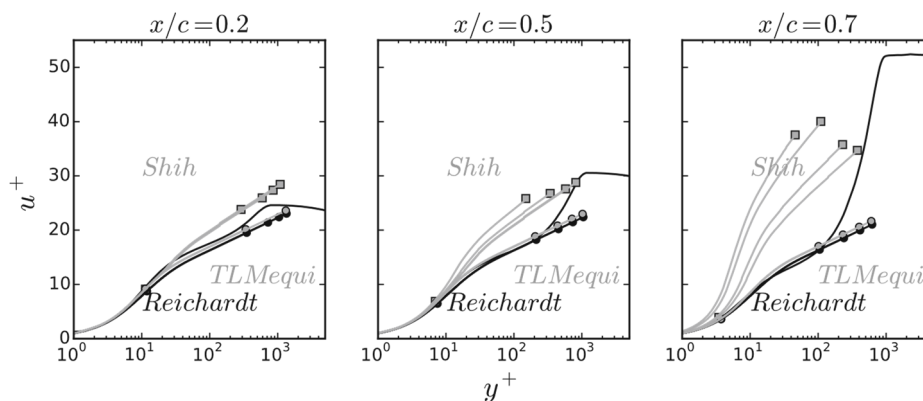


Fig. 14 Comparison in wall units and logarithmic scale of the velocity profiles estimated by three wallmodels to the wrLES data (solid black line) at three different chordwise locations. The markers show the position of the wall-model input. Wall-models that assume an equilibrium state are marked by circles with Reichardt (black) and TLMequi (gray). Shih's model that adds the contribution of the pressure-gradient is marked by gray squares

Table 2 Comparison of the shear stress estimated by the wall-models to the wrLES data $\frac{u_{\tau}(wm)-u_{\tau}}{u_{\tau}}$

	$x/c = 0.2$			$x/c = 0.5$			$x/c = 0.7$		
y/c	0.003	0.006	0.009	0.003	0.006	0.009	0.003	0.006	0.009
y^+	300	600	900	200	400	600	100	200	300
Reichardt	-20	-10	-20	-30	-20	0	-30	-10	20
TLMequi	10	n.c.	n.c.	0	10	30	-10	20	70
Werner-Wengle	20	20	20	0	10	20	-10	10	30
Shih	-50	-40	-40	-60	-50	-40	-90	-80	-60
TLMdp	-10	-110	-110	-110	-110	-120	-150	-210	n.c.

The error is given for three chordwise locations ($x/c = 0.2, 0.5$ and 0.7) and three wall-normal distances ($y/c \approx 3 \times 10^{-3}, 6 \times 10^{-3}$ and 9×10^{-3}). For more clarity, the wall-normal distances are rounded to one significant digit and the errors are rounded to 10

Although it is interesting to compare the velocity profiles obtained with the different models, the only critical output of the wall-model is the wall shear stress. Table 2 compares the shear velocity $u_{\tau}(wm)$ obtained with the five models to the wrLES shear velocity u_{τ} . It appears that Reichardt, Werner and Wengle and TLMequi models, namely the models assuming an equilibrium flow, provide results that are very close to each other. At $x/c = 0.2$ their error is smaller than 20% for the three input positions. At $x/c = 0.5$ and $x/c = 0.7$, the error stays low but it increases slightly, up to 70% for the highest input locations where $y^+ \geq 300$. This confirms what was observed previously: an equilibrium model can be used to model a flow submitted to an APG as long as the input position stays below the end of the log-region. Here, the most restrictive case in term of y^+ is at $x/c = 0.7$ where the log-region stops at $y^+ \approx 100$. This corresponds to $y/c \approx 0.003$, which is already more than 100 times larger than the current wrLES wall-normal mesh. It also appears, in Table 2, that the two models that solely consider the pressure-gradient (Shih and TLMdp) overestimate the impact of the APG and underestimate the shear. Their error is almost always larger than for the equilibrium models, with values ranging between 40% and 210%.

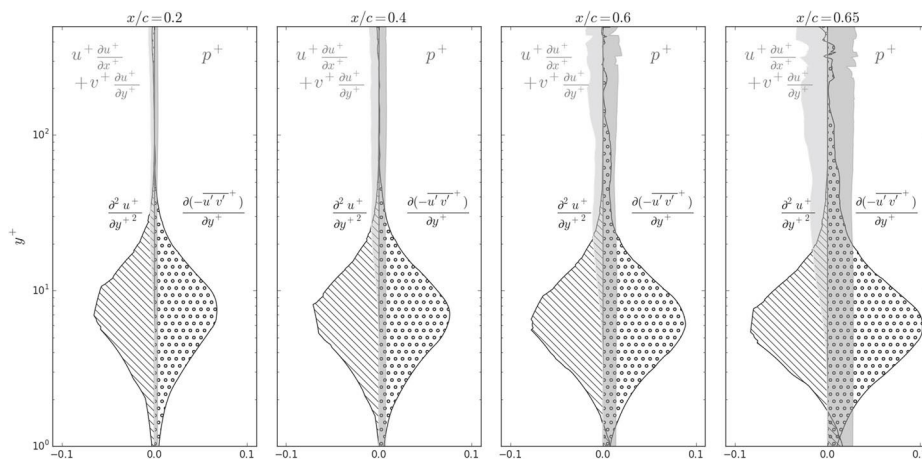


Fig. 15 Balance along the chord and along the wall-distance of the convective (light gray), pressure-gradient (dark gray) and left-hand side terms (hatched and dotted) considered in the TLM (4)

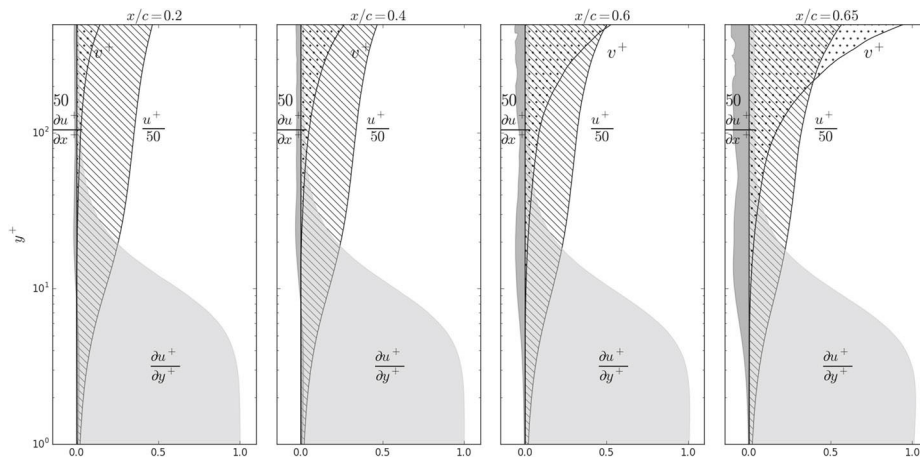


Fig. 16 Balance along the chord and along the wall-distance of the convective terms: u^+ (hatched), v^+ (dotted), $\frac{\partial u^+}{\partial x^+}$ (dark gray), and $\frac{\partial u^+}{\partial y^+}$ (light gray). Note that, to appear on the same scale, u^+ has been divided by 50, and $\frac{\partial u^+}{\partial x^+}$ multiplied by 50

Figure 15 presents a balance of the TLM terms along the chord at four positions between $x/c = 0.2$ and $x/c = 0.65$. Although the two terms that compose the left hand side term of the TLM equation ($\frac{\partial^2 u^+}{\partial y^{+2}}$ and $\frac{\partial(-u'v')}{\partial y^+}$) stay of the same order of magnitude at the different chordwise locations, both the pressure-gradient and the convective terms increase largely. At all the chordwise locations, as soon as y^+ is of 30 or so, the pressure-gradient and the convective terms essentially balance each other. Hence, if the convective terms are neglected in the TLM, the pressure-gradient term should be neglected as well. Note that, as for Fig. 12, the oscillations that appear on this figure are most likely due to the fact that the mesh is too coarse in that region, as discussed in Section 2.

If one wants to keep the pressure-gradient term but does not want to pay for the convective term calculation, a possible solution is to assume the evolution of the convective terms between the wall and the wall-model input location. One interesting option suggested by Berger and Aftosmis [40] is to use the value of the convective terms at the input location y_{wm} and to assume that they grow proportionally to the tangential velocity. Examining the different terms that compose the convective terms on Fig. 16, another option could be to assume a linear increase of the normal velocity and a constant streamwise velocity gradient. These two options will be tested in a future work.

6 Conclusion and Perspectives

In the present work, a wall-resolved LES of the NACA4412 at $Re = 1.64 \times 10^6$ and $\alpha = 12.0^\circ$ was performed in order to increase the understanding of the non-equilibrium boundary layer and to aid the development of wall-modeled LES.

The present wrLES results, obtained using a relatively small span, have been successfully compared to seven different numerical and experimental previous studies, in terms of pressure coefficient distribution, velocity and Reynolds stresses profiles. It appears that the obtained results are well within the range of the previous studies and also match well the experimental results.

An a priori analysis of the wall-models on the basis of the wrLES results was performed, showing that basic wall-model as Reichardt's law-of-the-wall or Werner and Wengle's model can be sufficient, as long as the

intercept is located well below the end of the log layer. More elaborate analytical models that take the pressure gradient into account, such as that proposed by Shih, do not seem appropriate for high Reynolds number flows. Finally, an analysis of the TLM terms as they appear in the wrLES confirms previous observations that the convective terms are almost balanced by the pressure-gradient term within the loglayer. This indicates that, also for the TLM, an equilibrium approach outperforms a more elaborate approach that is solely enriched by the pressure-gradient.

The wrLES used in this study was performed on a narrow span corresponding to 1% of the chord. This span is however adequate for the development of the turbulent boundary layer, and is therefore sufficient to perform wall-model comparison, as discussed in Section 2. In order to be more physically correct, further studies are currently performed on a span ten times larger.

This new computation will provide an evaluation of the span extent impact. It will also push the study further by comparing other models and by studying them based on timeaveraged data, as in the present work, but also based on instantaneous data.

Acknowledgments

The first author thanks Prof. Piomelli and Prof. Schlatter for the fruitful discussions during DLES11 conference, as well as J.-S. Cagnone, A. Johnen, M. Rasquin and J. Lacabanne for their judicious advices and support in the analysis, meshing, and post-processing of this work. She also would like to thank the reviewers for their thorough analyses of the text and their insightful remarks.

Funding information

This research has been financed by the Walloon Region through the FirstDoCA framework (grant number ECV320600FD016F/1217882). The study benefited from computational resources made available on the Tier-1 supercomputer of the Fédération Wallonie-Bruxelles (n°1117545).

REFERENCES

1. Breuer, M., Kniazev, B., Abel, M.: Development of wall models for LES of separated flows using statistical evaluations. *Comput. Fluids* 36(5), 817–837 (2007)
2. Cabot, W., Moin, P.: Approximate wall boundary conditions in the Large-Eddy simulation of high Reynolds number flow. *Flow Turbul. Combust.* 63, 269–291 (2000)
3. Kawai, S., Larsson, J.: Wall-modeling in large eddy simulation: length scales, grid resolution, and accuracy. *Phys. Fluids* 24(1), 015105 (2012)
4. Larsson, J., Kawai, S., Bodart, J., Bermejo-Moreno, I.: Large eddy simulation with modeled wall-stress: recent progress and future directions. *Mech. Eng. Rev.* 3(1), 15–00418 (2016). <https://doi.org/10.1299/mer.15-00418>
5. Piomelli, U.: *Wall-Modeled Large-Eddy Simulations: Present Status and Prospects*. Springer, Netherlands (2010)
6. Bose, S., Moin, P.: A dynamic slip boundary condition for wall-modeled large-eddy simulation. *Phys. Fluids* 26(1), 015104 (2014)
7. Frère, A., Sørensen, N.N., Hillewaert, K., Chatelain, P., Winckelmans, G.: Discontinuous galerkin methodology for large-eddy simulations of wind turbine airfoils. *Journal of Physics: Conference Series* 753(022037). <https://doi.org/10.1088/1742-6596/753/2/022037> (2016)

8. Park, G.I., Moin, P.: An improved dynamic non-equilibrium wall-model for large eddy simulation. *Phys.Fluids* 26(1), 015108 (2014)
9. Carton de Wiart, C., Murman, S.M.: Assessment of wall-modeled LES strategies within a discontinuous-Galerkin spectral-element framework. In: 55th AIAA Aerospace Sciences Meeting, pp. 1223 (2017)
10. Direct Numerical Simulations of channel flow over a smooth geometry (Dataset: “DNS channel flow with APG”). TurbBase Cineca IRODS repository, data creator: Laval, J.-P.
11. Bernard, A., Foucaut, J., Dupont, P., Stanislas, M.: Decelerating boundary layer: a new scaling and mixing length model. *AIAA J.* 41(2), 248–255 (2003)
12. Marquillies, M., Laval, J.P., Dolganov, R.: Direct numerical simulation of a separated channel flow with a smooth profile. *Journal of Turbulence* 9(N1) (2008)
13. Schlichting, H.: *Boundary Layer Theory*, 7th edn. Series in Mechanical Engineering, McGraw-Hill(1979)
14. ANSYS Fluent Theory Guide: 4.14.9 LES Near-Wall Treatment. https://www.sharcnet.ca/Software/Ansys/16.2.3/en-us/help/flu_th/flu_th.html (2015)
15. Werner, H., Wengle, H.: Large-Eddy Simulation of Turbulent Flow over and around a Cube in a Plate Channel. In: *Turbulent Shear Flows 8*. Springer, pp. 155–168 (1993)
16. Brionnaud, R., Holmann, D.M., Modena, M.C.: Aerodynamic analysis of the 2nd AIAA High Lift Prediction Workshop by a Lattice-Boltzmann Method solver (2014)
17. Shih, T.H., Povinelli, L.A., Liu, N.S., Potapczuk, M.G., Lumley, J.L.: A generalized wall function. Technical. Report. TM-1999-209398, National Aeronautics and Space Administration Glenn Research Center (1999)
18. Balaras, E., Benocci, C., Piomelli, U.: Two-layer approximate boundary conditions for large-eddy simulations. *AIAA J.* 34(6), 1111–1119 (1996)
19. Duprat, C., Balarac, G., Métais, O., Congedo, P.M., Brugière, O.: A wall-layer model for large-eddy simulations of turbulent flows with/out pressure gradient. *Phys. Fluids* 23(1), 015101 (2011). <https://doi.org/10.1063/1.3529358>
20. Hillewaert, K.: Development of the Discontinuous Galerkin Method for High-Resolution, Large Scale CFD and Acoustics in Industrial Geometries. Ph.D. thesis, Ecole polytechnique de Louvain/iMMC (2013)
21. Carton de Wiart, C., Hillewaert, K., Duponcheel, M., Winckelmans, G.: Assessment of a discontinuous Galerkin method for the simulation of vortical flows at high Reynolds number. *Int. J. Numer. Meth. Fluids* 74, 469–493 (2013). <https://doi.org/10.1002/flid.3859>
22. Frère, A., Hillewaert, K., Sarlak, H., Mikkelsen, R.F., Chatelain, P.: Cross-validation of numerical and experimental studies of transitional airfoil performance. In: *Proceedings-33Rd Wind Energy Symposium*. AIAA, Kissimmee (2015)
23. Carton de Wiart, C., Hillewaert, K., Bricteux, L., Winckelmans, G.: LES using a discontinuous Galerkin Method: isotropic turbulence, channel flow and periodic flow. In: *Proceedings of the ERCOFTAC Workshop “Direct and Large-Eddy Simulation 9”*. ERCOFTAC, Dresden (2013)
24. Frère, A., Carton de Wiart, C., Hillewaert, K., Chatelain, P., Winckelmans, G.: Application of wall-models to discontinuous Galerkin LES. *Phys. Fluids* 29(8), 085111 (2017)
25. Geuzaine, C., Remacle, J.F.: Gmsh: a three-dimensional finite element mesh generator with built-in pre- and post-processing facilities. *Int. J. Numer. Methods Eng.* 79(11), 1309–1331 (2009)
26. Langley Research Center Turbulence Modeling Resource: 2D NACA 4412 Airfoil Trailing Edge Separation (2DN44). Turbmodels.larc.nasa.gov
27. Choi, H., Moin, P.: Grid-point requirements for large eddy simulation: Chapman’s estimates revisited. *Phys. Fluids* 24(1), 011702 (2012)

28. Carton de Wiart, C.: Towards a Discontinuous Galerkin Solver for Scale-Resolving Simulations of Moderate Reynolds Number Flows, and Application to Industrial Cases. Ph.D. thesis, Ecole polytechnique de Louvain/iMMC (2014)
29. Drosson, M., Hillewaert, K., Essers, J.A.: Stability and boundary resolution analysis of the discontinuous Galerkin method applied to the Reynolds-averaged Navier–Stokes equations using the Spalart–Allmaras model. *SIAM J. Sci. Comput.* 35(3), B666–B700 (2013)
30. Wadcock, A.J.: Investigation of low-speed turbulent separated flow around airfoils. Nasa - 177450 NASA Ames Research Center (1987)
31. Hastings, R., Williams, B.: Studies of the flow field near a NACA 4412 airfoil at nearly maximum lift. *Aeronaut. J.* 91(901), 29–44 (1987)
32. Jansen, K.: Preliminary large-eddy simulations of flow around a naca 4412 airfoil using unstructured grids. Annual Research Briefs, Center for Turbulence Research Stanford university/NASA Ames Research Center (1995)
33. Jansen, K.: Large-eddy simulation of flow around a naca 4412 airfoil using unstructured grids. Annual Research Briefs, Center for Turbulence Research. Stanford University/NASA Ames Research Center, pp. 225–232 (1996)
34. Kaltenbach, H.J., Choi, H.: Large-Eddy Simulation of Flow around an Airfoil on a Structured Mesh. Center for Turbulence Research, Annual Research Briefs (1995)
35. Schmidt, S., Franke, M., Thiele, F.: Assessment of SGS models in Les applied to a Naca 4412 airfoil. In: 39th AIAA Aerospace Sciences Meeting and Exhibit (2001)
36. Venugopal, P., Cheung, L., Jothiprasad, G., Lele, S.: Large Eddy simulation of a wind turbine airfoil at high angle of attack. In: Center for Turbulence Research Proceedings of the Summer Program 2012 (2012)
37. Vinuesa, R., Hosseini, S.M., Hanifi, A., Henningson, D.S., Schlatter, P.: Pressure-gradient turbulent boundary layers developing around a wing section. *Flow Turbul. Combust.* 99(3-4), 613–641 (2017)
38. Chen, Z.L., Hickel, S., Devesa, A., Berland, J., Adams, N.A.: Wall modeling for implicit large-eddy simulation and immersed-interface methods. *Theor. Comput. Fluid Dyn.* 28(1), 1–21 (2014). <https://doi.org/10.1007/s00162-012-0286-6>
39. Wang, M., Moin, P.: Dynamic wall modeling for large-eddy simulation of complex turbulent flows. *Phys. Fluids* 14(7), 2043–2051 (2002)
40. Berger, M.J., Aftosmis, M.J.: An ODE-based wall model for turbulent flow simulations. *AIAA J.* 56(2), 700–714 (2018)